

Propagation characteristics of ultrasonic guided waves in tram rails

Kui Sun^a, Hua-peng Chen* Qingsong Feng^b and Xiaoyan Lei^b

Engineering Research Center of Railway Environment Vibration and Noise, Ministry of Education, East China Jiao Tong University, Nanchang, 330013, China

(Received February 1, 2020, Revised April 3, 2020, Accepted April 18, 2020)

Abstract. Ultrasonic guided wave testing is a very promising non-destructive testing method for rails, which is of great significance for ensuring the safe operation of railways. On the basis of the semi-analytical finite element (SAFE) method, an analytical model of 59R2 grooved rail was proposed, which is commonly used in the ballastless track of modern tram. The dispersion curves of ultrasonic guided waves in free rail and supported rail were obtained. Sensitivity analysis was then undertaken to evaluate the effect of rail elastic modulus on the phase velocity and group velocity dispersion curves of ultrasonic guided waves. The optimal guided wave mode, optimal excitation point and excitation direction suitable for detecting rail integrity were identified by analyzing the frequency, number of modes, and mode shapes. A sinusoidal signal modulated by a Hanning window with a center frequency of 25 kHz was used as the excitation source, and the propagation characteristics of high-frequency ultrasonic guided waves in the rail were obtained. The results show that the rail pad has a relatively little influence on the dispersion curves of ultrasonic guided waves in the high frequency band, and has a relatively large influence on the dispersion curves of ultrasonic guided waves in the low frequency band below 4 kHz. The rail elastic modulus has significant influence on the phase velocity in the high frequency band, while the group velocity is greatly affected by the rail elastic modulus in the low frequency band.

Keywords: guided wave; tram rail; phase velocity; group velocity; wave propagation

1. Introduction

As an important part of the railway transportation system, the condition of the rails directly affects the safety of railway operation. Since the rail directly bears the pressure from the wheel, rail fracture caused by fatigue cracks and defects will lead to major accidents such as derailment and overturning of the train (Chen and Zhang 2017, Panunzio *et al.* 2018, Lu *et al.* 2018, Zhang *et al.* 2015). If the rail damage can be detected and located in the early stage, the occurrence of major accidents can be avoided. With the increase of the railway traffic density and the running speed, the load and impact of the rail increases, and the probability of rail failure increases, which further challenges the traditional rail damage detection and health monitoring technology. As a useful type of non-destructive testing technology, ultrasonic guided wave has particular advantages for large-scale rail defect detection due to its long propagation distance and high detection efficiency (Chen 2018, Dziejch *et al.* 2016, Uyar and Babayigit 2016). Therefore, guided wave detection technology for rail is also a hot issue in the field of non-destructive testing in the world.

In order to find rail defects in time and ensure the safety of railway transportation, extensive researches have been

undertaken on rail nondestructive testing. Rose *et al.* (2004a) studied the propagation of guided waves at the rail head using ABAQUS finite element simulation software. Also, the 60 kHz Lamb wave and SH wave were excited by the pulse hammer-air coupling ultrasonic transducer and EMAT transducer at the rail head. The detection of track head damage by the one-sending-one-receiving method and the pulse echo method was studied. Coccia *et al.* (2011) analyzed the guide wave dispersion characteristics of the rail head and the guided wave modes excited by symmetric and asymmetric loading modes by the SAFE method. Rizzo *et al.* (2010) used a laser-air coupled ultrasonic transducer to excite guided waves at the rail head and received echoes. Then the discrete wavelet transform algorithm was used to achieve the feature extraction of the echo signals. Cemiglia *et al.* (2012) studied the relationship between the propagation characteristics of guided waves at the rail bottom and those in the plate structure by experimental methods. Bartoli *et al.* (2006) investigated the attenuation laws of different modal guided waves in rails in detail by the SAFE method. Gharaibeh *et al.* (2011) studied the characteristics of different modes of guided waves in rail, and designed piezoelectric transducer array to realize the excitation of specific modes of guided waves. Ramatolo *et al.* (2018) proposed a coupling method of semi analytical method and three-dimensional finite element to simulate the propagation of guided wave in rail. In the existing studies, the I-shaped rails commonly used in high-speed railways, ordinary-speed railways and heavy-duty railways are typically considered, while the research on the 59R2 grooved rails commonly used in modern trams is limited. Also, the influence of rail pad on the dispersion curve of

*Corresponding author, Professor

E-mail: hp.chen@ecjtu.edu.cn; hp.chen@outlook.com

^a Ph.D. Student

E-mail: kui_sun@outlook.com

^b Professor

guided wave has not been investigated in most studies. Therefore, it is of great engineering and practical significance to study the dispersion curves and propagation characteristics of guided waves for 59R2 grooved rails.

In this paper, the analytical model of 59R2 grooved rail is constructed by the SAFE method, and the dispersion curves of guided wave phase velocity and group velocity in free rail and supported rail are obtained. The effects of rail elastic modulus on low-frequency and high-frequency guided wave phase velocity and group velocity are analyzed in detail. Based on the frequency selection factor, the optimal excitation frequency of rail guided wave is determined, and the guided wave mode, the optimal excitation point and the excitation direction suitable for on-site detection are selected by modal analysis. Finally, the sinusoidal signal modulated by the Hanning window is used as the excitation source, and the propagation characteristics of the high-frequency ultrasonic guided wave in the rail are analyzed.

2. Semi-analytical finite element model

2.1 Governing equations

The SAFE method is a semi-analytical method for solving the dispersion problem in a complex cross-section waveguide medium. When this method is used to solve the dispersion solution, only the cross section of the waveguide medium needs to be discretized by the finite element method, and the displacement along the propagation direction of the waveguide medium is represented by the vibration of the simple harmonic wave (Duan *et al.* 2017, Hayashi *et al.* 2003, Li *et al.* 2015). The prism element is used to discrete the elastic body, which consists of small quadrilaterals on the x-y plane and straight edges in the z direction. According to the principle of virtual work, the governing equation is as follows

$$\int_{\Gamma} \delta \mathbf{u}^T \mathbf{t} d\Gamma = \int_V \delta \mathbf{u}^T (\rho \ddot{\mathbf{u}}) dV + \int_V \delta \boldsymbol{\varepsilon}^T \boldsymbol{\sigma} dV \quad (1)$$

where \mathbf{u} , $\boldsymbol{\varepsilon}$, $\boldsymbol{\sigma}$, and \mathbf{t} are displacement vector, strain vector, stress vector, and external load vector, respectively, of the element; ρ is material density; $\int_{\Gamma} \bullet d\Gamma$ and $\int_V \bullet dV$ represent the area and volume integral of prismatic elements, respectively.

Furthermore, it is assumed that any point on the elastic body is subjected to simple harmonic vibration, then the displacement vector of a point on the elastic body can be written as

$$\mathbf{u} = \mathbf{N}(x, y) \mathbf{U}^j(z) \exp(-i\omega t) \quad (2)$$

where $\mathbf{N}(x, y)$ is interpolation function; $\mathbf{U}^j(z)$ is the nodal displacement vector of the j th element; and $i = \sqrt{-1}$.

Since $\mathbf{U}^j(z)$ is only a function of z , according to the inverse Fourier transform, $\mathbf{U}^j(z)$ can be rewritten as

$$\mathbf{U}^j(z) = \int_{-\infty}^{+\infty} \bar{\mathbf{U}}^j \exp(i\xi z) d\xi \quad (3)$$

At a certain wave number ξ , the nodal displacement vector of any point on the j th element can be expressed as

$$\mathbf{u} = \mathbf{N}(x, y) \bar{\mathbf{U}}^j(z) \exp(i\xi z - i\omega t) \quad (4)$$

The strain vector $\boldsymbol{\varepsilon}$ can be given by the displacement vector as

$$\boldsymbol{\varepsilon} = \left[\mathbf{L}_x \frac{\partial}{\partial x} + \mathbf{L}_y \frac{\partial}{\partial y} + \mathbf{L}_z \frac{\partial}{\partial z} \right] \mathbf{u} \quad (5)$$

$$\mathbf{L}_x = \begin{bmatrix} 1 & 0 & 0 \\ 0 & 0 & 0 \\ 0 & 0 & 0 \\ 0 & 0 & 0 \\ 0 & 0 & 1 \\ 0 & 1 & 0 \end{bmatrix}, \quad \mathbf{L}_y = \begin{bmatrix} 0 & 0 & 0 \\ 0 & 1 & 0 \\ 0 & 0 & 0 \\ 0 & 0 & 1 \\ 0 & 0 & 0 \\ 1 & 0 & 0 \end{bmatrix}, \quad (6)$$

$$\mathbf{L}_z = \begin{bmatrix} 0 & 0 & 0 \\ 0 & 0 & 0 \\ 0 & 0 & 1 \\ 0 & 1 & 0 \\ 1 & 0 & 0 \\ 0 & 0 & 0 \end{bmatrix}.$$

Substituting Eq. (4) into Eq. (5) yields

$$\boldsymbol{\varepsilon} = (\mathbf{B}_1 + i\xi \mathbf{B}_2) \bar{\mathbf{U}}^j \exp(i\xi z - i\omega t) \quad (7)$$

$$\mathbf{B}_1 = \mathbf{L}_x \mathbf{N}_{,x} + \mathbf{L}_y \mathbf{N}_{,y}, \quad \mathbf{B}_2 = \mathbf{L}_z \mathbf{N} \quad (8)$$

where $\mathbf{N}_{,x}$ and $\mathbf{N}_{,y}$ are partial derivatives of the interpolation function \mathbf{N} for x and y , respectively.

According to the stress-strain relationship of linear elastic materials, the stress vector $\boldsymbol{\sigma}$ can be expressed as

$$\boldsymbol{\sigma} = \mathbf{D} \boldsymbol{\varepsilon} \quad (9)$$

where \mathbf{D} is elastic matrix.

Similar to the displacement vector \mathbf{u} in Eq. (4), the external load vector \mathbf{t} can be represented by the nodal traction vector $\bar{\mathbf{T}}^j$ as

$$\mathbf{t} = \mathbf{N} \bar{\mathbf{T}}^j \exp(i\xi z - i\omega t) \quad (10)$$

Substituting Eq. (4), Eq. (7), Eq. (9), and Eq. (10) into Eq. (1), leads to

$$\mathbf{f}^j = (\mathbf{K}_1^j + i\xi \mathbf{K}_2^j + \xi^2 \mathbf{K}_3^j) \bar{\mathbf{U}}^j - \omega^2 \mathbf{M}^j \bar{\mathbf{U}}^j \quad (11)$$

$$\begin{aligned} \mathbf{K}_1^j &= \int_y \int_x \mathbf{B}_1^T \mathbf{D} \mathbf{B}_1 dx dy, \mathbf{K}_2^j \\ &= \int_y \int_x (\mathbf{B}_1^T \mathbf{D} \mathbf{B}_2 - \mathbf{B}_2^T \mathbf{D} \mathbf{B}_1) dx dy, \mathbf{K}_3^j \\ &= \int_y \int_x \mathbf{B}_2^T \mathbf{D} \mathbf{B}_2 dx dy. \end{aligned} \quad (12)$$

$$\mathbf{f}^j = \int_{\Gamma'} \mathbf{N}^T \mathbf{N} \bar{\mathbf{T}}^j d\Gamma', \mathbf{M}^j = \int_y \int_x \rho \mathbf{N}^T \mathbf{N} dx dy. \quad (13)$$

where \mathbf{K}_1^j , \mathbf{K}_2^j and \mathbf{K}_3^j are the stiffness matrix of the j th element, respectively; \mathbf{f}^j is the nodal force vector of the j th element; \mathbf{M}^j is the mass matrix of the j th element; Γ' is the boundary of cross section.

Through numerical integration, the stiffness matrices and the nodal force vector in Eqs. (12-13) can be obtained, then the related system matrices assembled by the corresponding matrices of each element can be given. Thus, the control equation of the whole system can be written as

$$(\mathbf{K}_1 + i\xi\mathbf{K}_2 + \xi^2\mathbf{K}_3 - \omega^2\mathbf{M})\bar{\mathbf{U}} = \mathbf{f} \quad (14)$$

where \mathbf{K}_1 , \mathbf{K}_2 , \mathbf{K}_3 and \mathbf{M} are system stiffness and mass matrices with dimensional of the $M \times M$ (M is three times the total number of nodes); \mathbf{f} is the $M \times 1$ nodal force vector; $\bar{\mathbf{U}}$ is the unknown node displacement vector.

2.2 Phase velocity and group velocity

Assuming $\mathbf{f} = 0$, the free vibration equation of the structure system is

$$(\mathbf{K}_1 + i\xi\mathbf{K}_2 + \xi^2\mathbf{K}_3 - \omega^2\mathbf{M})\bar{\mathbf{U}} = 0 \quad (15)$$

If $\bar{\mathbf{U}}$ in Eq. (15) has a non-zero solution, the determinant of coefficient matrix must be zero, that is

$$\det(\mathbf{K}_1 + i\xi\mathbf{K}_2 + \xi^2\mathbf{K}_3 - \omega^2\mathbf{M}) = 0 \quad (16)$$

When the frequency ω is given, the corresponding eigenvalue ξ_m ($m = 1, 2, \dots, 2M$) can be obtained by Eq. (16). From the mathematical point of view, Eq. (15) defines a quadratic eigenvalue problem in the complex number field. The number of feature pairs (eigenvalues and eigenvectors) is equal to twice the degrees of freedom of the structural system. These eigenvalues include the wavenumber of waves traveling in the positive z direction and waves traveling in the negative z direction, respectively.

Since Eq. (15) contains imaginary terms $i\xi\mathbf{K}_2$, in order to facilitate the solution of the characteristic equation, an auxiliary matrix \mathbf{T} is introduced, that is

$$\mathbf{T} = \text{diag}(1 \ 1 \ i \ \dots \ 1 \ 1 \ i) \quad (17)$$

After introducing the auxiliary matrix \mathbf{T} , Eq. (15) becomes

$$(\mathbf{K}_1 + \xi\hat{\mathbf{K}}_2 + \xi^2\mathbf{K}_3 - \omega^2\mathbf{M})\hat{\mathbf{U}} = 0 \quad (18)$$

Furthermore, Eq. (18) can be written as a first-order eigenvalue problem, that is

$$(\mathbf{A} - \xi\mathbf{B})\mathbf{Q} = 0 \quad (19)$$

$$\mathbf{A} = \begin{bmatrix} 0 & \mathbf{K}_1 - \omega^2\mathbf{M} \\ \mathbf{K}_1 - \omega^2\mathbf{M} & \hat{\mathbf{K}}_2 \end{bmatrix}, \quad \mathbf{B} = \begin{bmatrix} \mathbf{K}_1 - \omega^2\mathbf{M} & 0 \\ 0 & -\mathbf{K}_3 \end{bmatrix} \quad (20)$$

$$\mathbf{Q} = \begin{bmatrix} \hat{\mathbf{U}} \\ \xi\hat{\mathbf{U}} \end{bmatrix}.$$

Since the imaginary number term has been eliminated in Eq. (19), the functions for solving the general first-order eigenvalue problem can be used, such as eig and eigs functions in MATLAB. By solving Eq. (19), the left eigenvalue vector $\hat{\mathbf{U}}_L$ ($1 \times 2M$) and the right eigenvalue vector $\hat{\mathbf{U}}_R$ ($2M \times 1$) can be obtained, respectively.

At a given frequency ω , the phase and group velocity of the m th mode is defined as

$$c_{pm} = \frac{\omega}{\xi_m} \quad (21)$$

The formula for calculating the group velocity of the m th mode is calculated from

$$c_g = \frac{\partial\omega}{\partial\xi} = \frac{\hat{\mathbf{U}}_L^T (\hat{\mathbf{K}}_2 + 2\xi\mathbf{K}_3) \hat{\mathbf{U}}_R}{2\omega \hat{\mathbf{U}}_L^T \mathbf{M} \hat{\mathbf{U}}_R} \quad (22)$$

When the characteristic Eq. (19) is solved, ω , ξ , $\hat{\mathbf{U}}_R$ and $\hat{\mathbf{U}}_L$ can be obtained, and then the group velocity dispersion curves of ultrasonic guided wave are obtained by using Eq. (22).

2.3 Displacement field

When the excitation signal is located at $z = z_s$, all the propagation modes inside the rail can be expressed as

$$\mathbf{U}_d(x, y, f) = \sum_{m=1}^{2M} -\frac{\Phi_m^L \tilde{\mathbf{p}}}{\mathbf{B}_m} \Phi_m^{Rup} e^{i[\xi_m(z-z_s)]} \quad (23)$$

$$\mathbf{B}_m = \Phi_m^L \mathbf{B} \Phi_m^R \quad (24)$$

where f is the frequency; m is the number of ultrasonic guided wave modes at frequency f , with a total of $2M$ modes; $\tilde{\mathbf{p}}$ is the amplitude of the excitation signal; Φ_m^L is the left eigenvector of the m th modal ultrasonic guided wave; Φ_m^{Rup} is the upper half of the right eigenvector Φ_m^R of the m th modal ultrasonic guided wave.

First, the Fourier transform is performed on the excitation signal $F(t)$, that is,

$$\hat{F}(f) = \int_{-\infty}^{+\infty} F(t) e^{-i2\pi ft} dt \quad (25)$$

Then, by convoluting with the nodal displacement vector, the excitation response function of position z_s is

$$\mathbf{V}(x, y, f) = \hat{F}(f) \cdot \mathbf{U}_d(x, y, f) \quad (26)$$

Finally, the time domain response obtained by the inverse Fourier transform is

$$\mathbf{V}(x, y, t) = \int_{-\infty}^{+\infty} \mathbf{V}(x, y, f) e^{i2\pi ft} df \quad (27)$$

3. Rail dispersion relations

3.1 Free rail

The rail profile used in this paper is a standard 59R2 section commonly used in ballastless track of modern trams. The three-node triangular element is used to

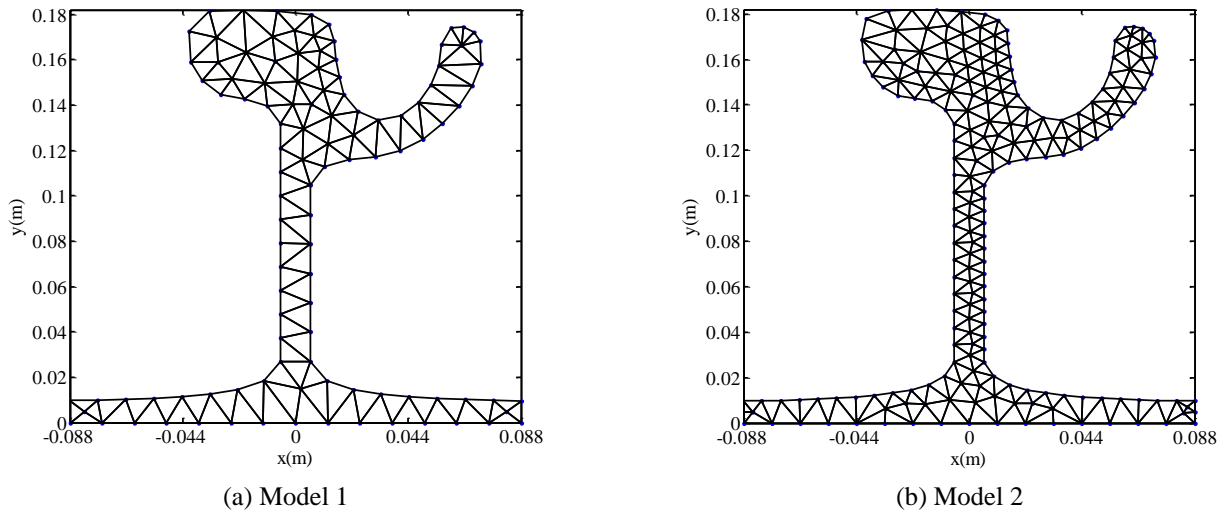


Fig. 1 Two model meshes for free rail

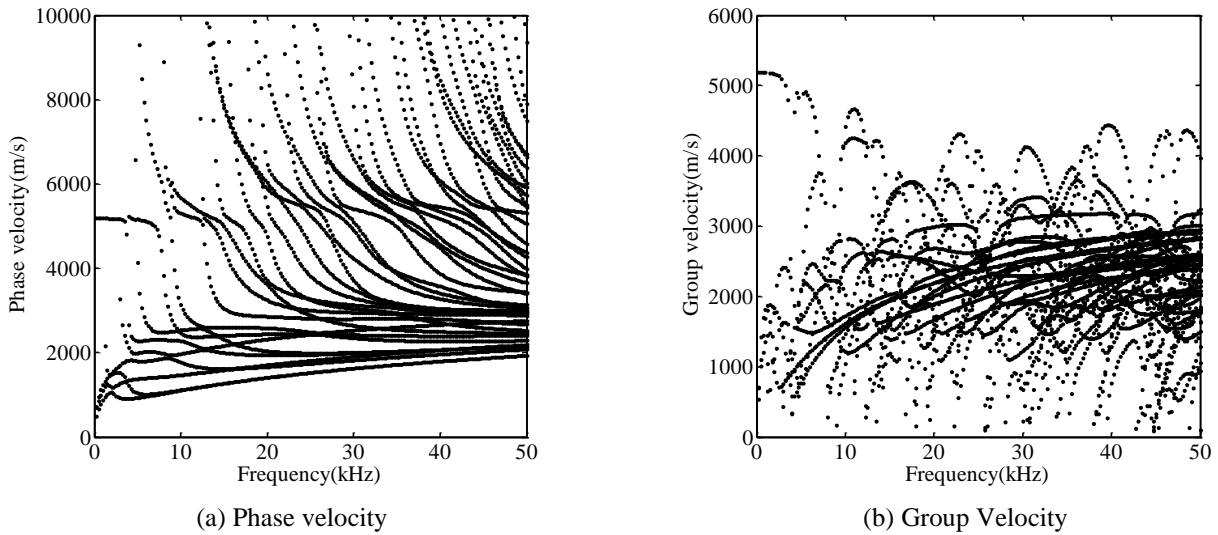


Fig. 2 Guided wave dispersion curves of free rail

discretize the cross section of the rail. Each element has 3 nodes and each node has three translational degrees of freedom. There are two different finite element meshes used, i.e. Model 1 and Model 2, as shown in Fig. 1. The element sizes of model 1 and model 2 are 0.01m and 0.006mm, respectively. Model 1 has 132 elements and 327 degrees of freedom, and Model 2 has 291 elements and 621 degrees of freedom. The rail is considered to be an isotropic material with density of 7800 kg/m³, elastic modulus of 210 GPa, and Poisson's ratio of 0.3. It should be pointed out that the width of the rail web is 0.012m.

On the basis of the SAFE method introduced in Section 2, the dispersion curves of phase velocity and group velocity of ultrasonic guided waves in two cases of mesh rails are obtained, respectively. The results show that the phase velocities and group velocities obtained by the two finite element meshes are generally identical, and the deviation of the results is within 0.5%. Therefore, the coarse finite element mesh Model 1 is used in the subsequent analysis. The phase and group velocity dispersion curves are shown in Fig. 2.

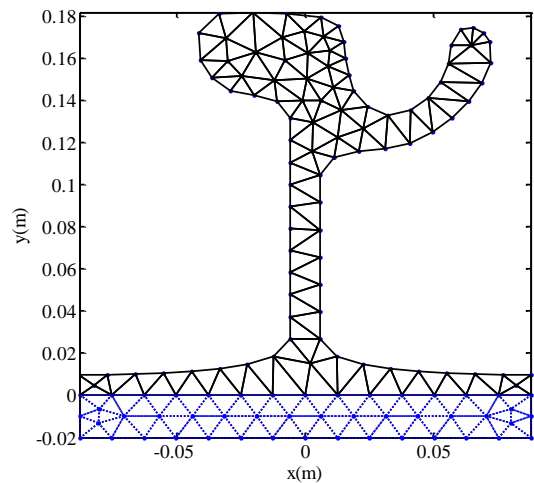


Fig. 3 Model mesh for supported rail

It can be seen from Fig. 2 that there are many complex guided wave modes in the rail due to the complex cross

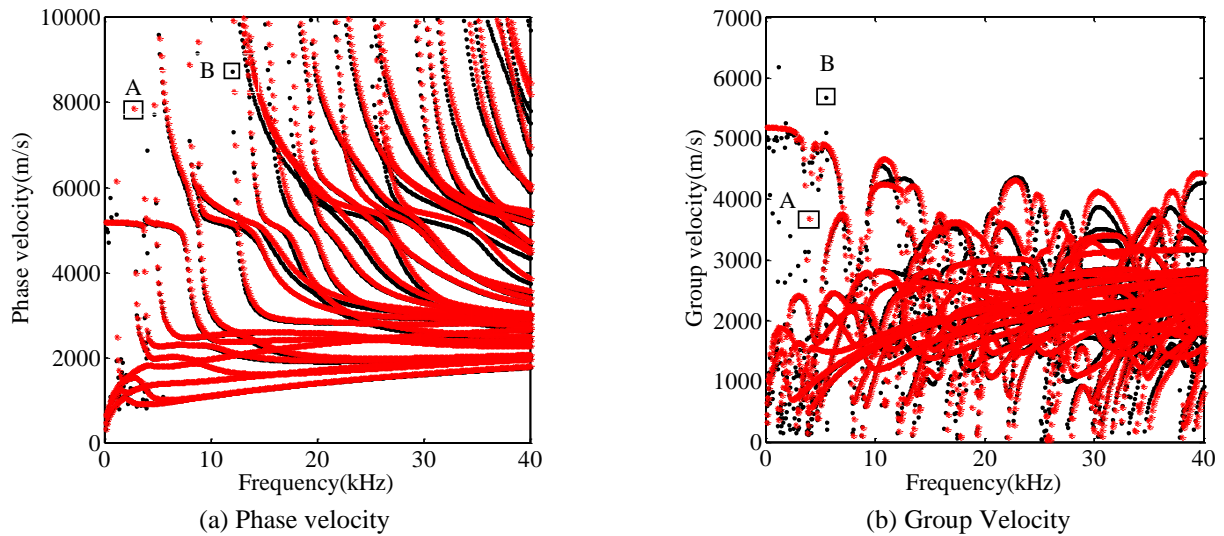


Fig. 4 Guided wave dispersion curves of free rail (A) and supported rail (B)

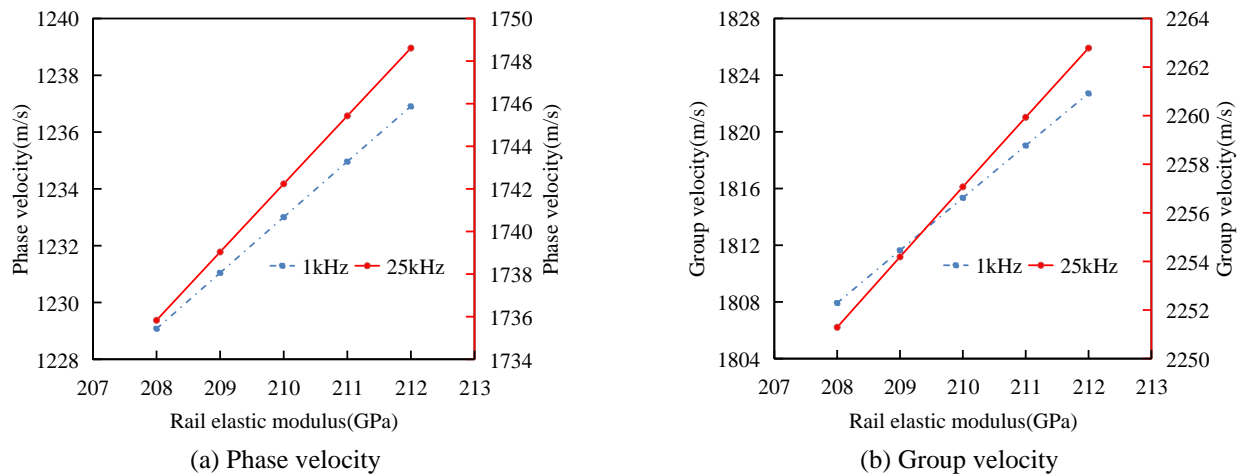


Fig. 5 Effect of rail elastic modulus on phase velocity and group velocity

section shape of 59R2 grooved rail. The rail has 9 guided wave modes at a frequency of 5 kHz and 44 guided wave modes at a frequency of 50 kHz. Therefore, as the frequency increases, the number of guided wave modes also gradually increases, and the propagation speed of different guided wave modes changes with the frequency, which indicates that the guided wave propagation in the 59R2 grooved rail has obvious multimodal and dispersion characteristics.

3.2 Supported rail

In the actual track structure, the rail is generally fixed by the rail pad with periodic discrete support. Therefore, the effect of the elastic pad on the dispersion curve of the rail guided wave is analyzed in this section. Due to the periodic discrete support characteristics of the rail pad, there is no guided wave propagating in the longitudinal direction in the rail pad. In order to simulate this phenomenon, the rail pad is considered as an orthotropic material (Nilsson *et al.* 2009, Ryue *et al.* 2008). In the elastic matrix, only the vertical elastic modulus of the rail pad is considered, and the shear

modulus and the elastic modulus in other directions are all taken as zero. The rails are still simulated with isotropic materials. The finite element model is shown in Fig. 3. The finite element mesh has 194 elements and 426 degrees of freedom.

The material of the rail pad is rubber. The vertical elastic modulus of the rail pad is 4MPa, the density is 1000kg/m³, and the Poisson's ratio is 0.45. The parameters used in the rail are the same as the above section. The dispersion curve of phase velocity and group velocity of the supported rail is shown in Fig. 4.

It can be seen from Fig. 4 that in the high frequency range of 5kHz-40kHz, the phase velocity and group velocity dispersion curve shapes of the supported rail and the free rail are very similar, but there is a certain speed deviation. However, in the low frequency band below 4kHz, the dispersion curves of the phase velocity and group velocity of the supported rail appear a little change. Therefore, the rail pad has a relatively little influence on the rail guide wave dispersion curves in the high frequency band, and a relatively large influence on the guide wave dispersion curves in the low frequency band below 4 kHz.

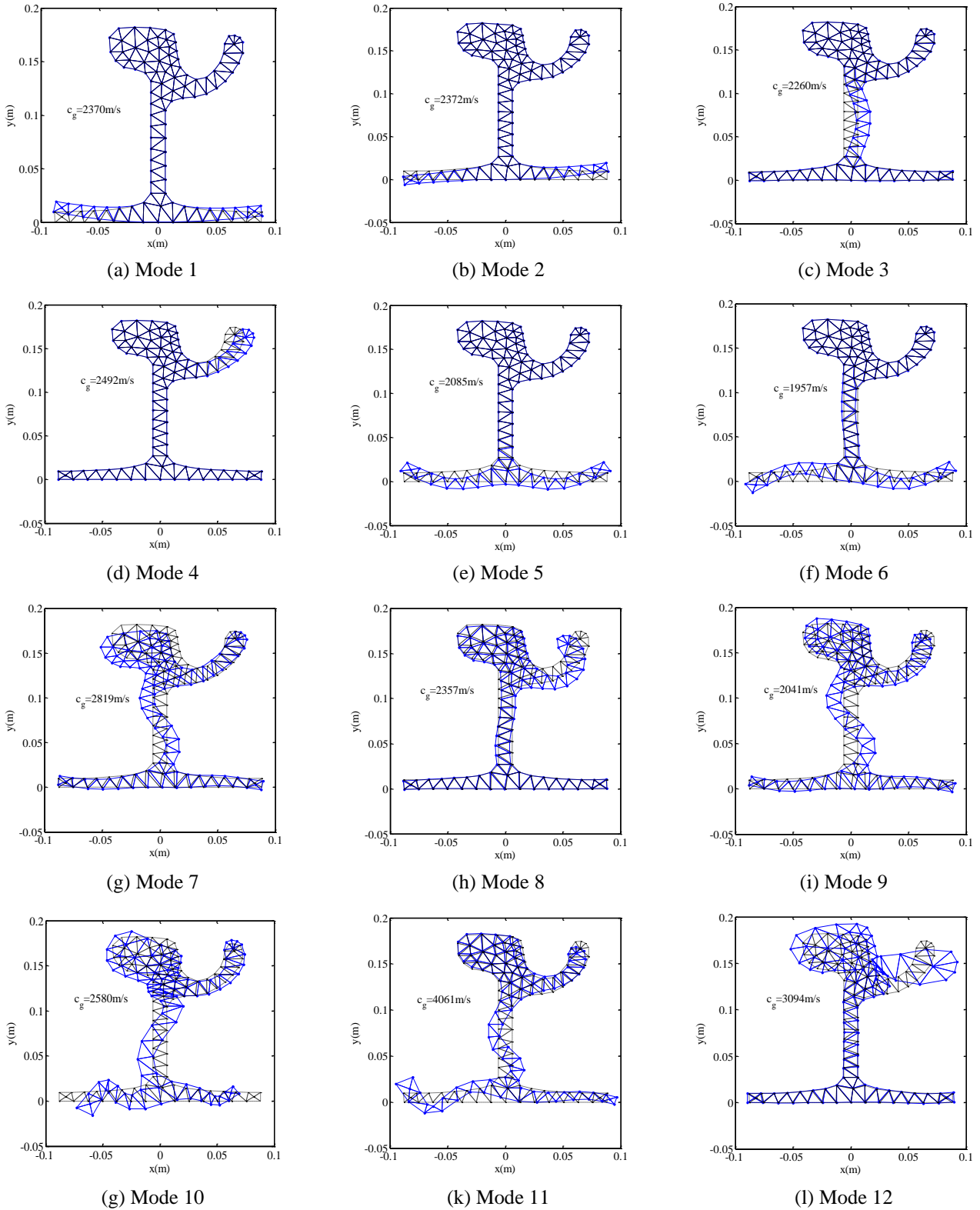


Fig. 6 Mode shapes of partial rail guided waves at 25kHz

3.3 Effects of rail elastic modulus

Rail temperature change of 1°C leads to elastic modulus change of 0.05GPa (Wang *et al.* 2018). It is assumed that the rail elastic modulus is 210 GPa at room temperature of

20°C. If the rail temperature varies from -20°C to 60°C, the elastic modulus varies from 208GPa to 212GPa. Fig. 5 shows the effect of elastic modulus variations on the phase and group velocities of the third-order guided wave mode for a 59R2 grooved rail.

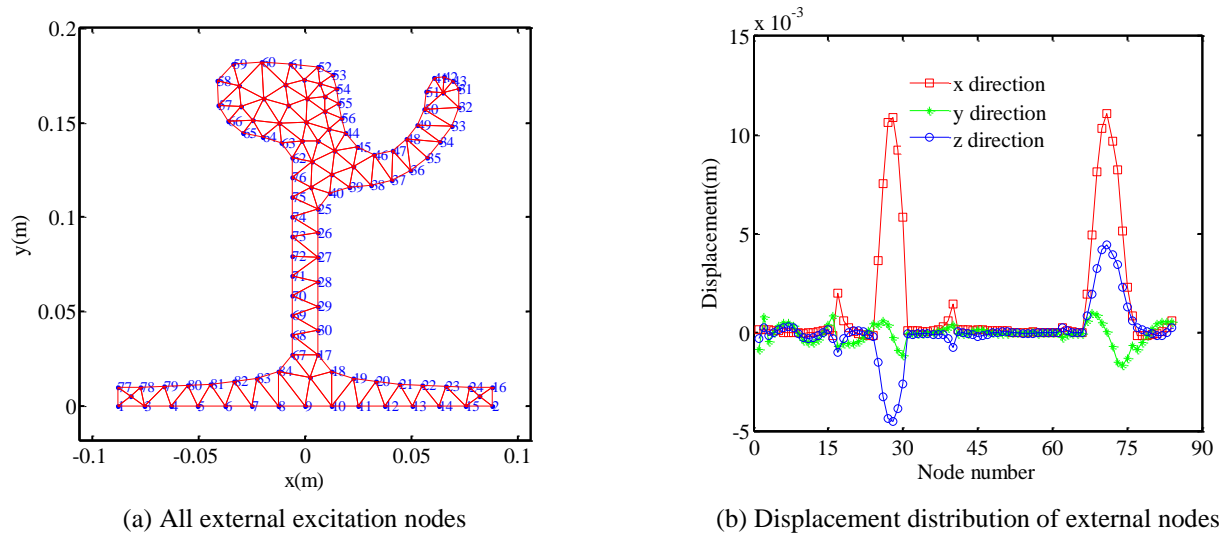


Fig. 7 Displacement of external nodes in the mode 3

It can be seen from Fig. 5 that with the increase of rail elastic modulus, both the phase velocity and group velocity of guided waves increase at the frequencies of 1kHz and 25kHz. The amplitudes of phase velocity variation in low and high frequency bands are 0.64% and 0.74%, respectively. The changes of group velocity in the low and high frequency bands are 0.82% and 0.51%, respectively. The results show that the phase velocity is greatly affected by the elastic modulus change in the high frequency range, while the group velocity is more affected by the elastic modulus change in the low frequency range.

4. Propagation characteristics of guided waves

4.1 Selection of mode and optimal excitation position

The eigenvector obtained by solving the rail guided wave dispersion curves represent the displacements at the rail cross-section nodes, that is, the mode shape of the guided wave mode. When selecting the guided wave mode for practical damage detection, the dispersion characteristics of the guided wave propagation in the waveguide structure and the modal displacements should be considered at the same time. Therefore, the mode shape is one of the important reference factors for the mode selection in guided wave detection (Rose *et al.* 2004b). The typical 12th-order mode shapes of rail guide wave at 25kHz are shown in Fig. 6.

It can be seen from the results in Fig. 6 that the maximum amplitude positions of various modes are quite different. Some of them have large amplitude at the rail head, some at the rail bottom, some at the rail head, rail web and rail bottom. When the guided waves of different modes propagate, the energy distribution in different positions of the rail is different. Therefore, the mode shape of the selected mode should have displacements in the direction of the damaged position, which is more suitable for detecting

the damage or stress in the rail structure (Hayashi 2018, Yao *et al.* 2017, Shi *et al.* 2019).

The displacements of mode 1, mode 2, mode 5 and mode 6 are mainly concentrated at the rail bottom. Considering the actual situation of continuous welded rail, the rail bottom is constrained by the fastener, thus its propagation distance will be greatly reduced. The mode shapes of modes 7-12 are complex. If these modes are selected for rail detection, multiple guided wave modes may be excited at the same time, which is not conducive to the later signal processing. The mode shapes of mode 3 and mode 4 are relatively simple, and the displacements are concentrated at the rail web and rail head, respectively. Since the position of the rail head is not convenient to install the ultrasonic guided wave transducers, the mode 3 is selected as the preferred mode in the damage detection of the 59R2 grooved rail.

Because the nodes inside the rail cross-section cannot be excited in reality, only the nodes outside the rail cross-section can be selected as alternative excitation points. There are 84 nodes in total, as shown in Fig. 7(a). Each node has three degrees of freedom, and the displacements of the external nodes of the mode 3 in the three degrees of freedom are plotted, as shown in Fig. 7(b).

The results in Fig. 7 shows that the displacement components of the mode 3 in the x and z directions are significantly larger than the displacement components in the y direction. The point with maximum displacement is the potential optimal excitation position. Therefore, the optimal excitation position of mode 3 is the x and z directions of node 28 and node 71.

4.2 Frequency selection

In the process of guided wave inspection, the excitation signal will cause energy dispersion due to multi-modality, and the dispersion characteristics of the guided wave will also increase the received signal bandwidth, which is not conducive to later signal processing and analysis (Xu *et al.*

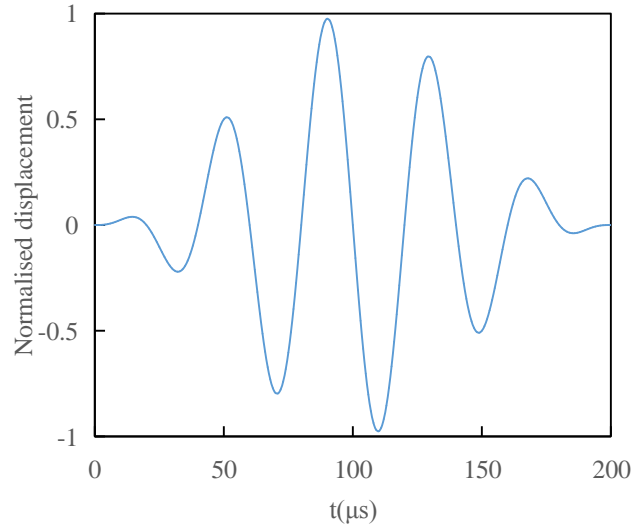


Fig. 8 Excitation signal

Table 1 Frequency selection factor

Frequency	22.5kHz	25kHz	30kHz	40kHz
Mode number	21	22	26	35
Velocity difference(m/s)	773	967	723	952
α	1.33	1.59	1.01	0.98

2018). Therefore, the following three factors need to be taken into account to select the appropriate detection frequency:

(1) The propagation group velocity of the selected guided wave mode is quite different from that of other modes. When the propagation speed of the guided wave signal is similar to that of other modal signals, the time domain signals of different modes will be superimposed, which makes it difficult to extract the signal in the later stage. The obvious difference of propagation speed is helpful to realize the modal separation of the detection signal and improve the sensitivity of detection.

(2) Guided wave modes should have good non-dispersive properties at a specific frequency, that is, the dispersion curve is relatively smooth near the frequency. Frequency dispersion has a great influence on the propagation distance of ultrasonic guided waves in a 59R2 grooved rail. When the guided wave signal propagates to a certain distance, the time domain signal amplitude will be significantly reduced, which will greatly reduce the sensitivity of damage or stress detection.

(3) When points (1) and (2) are satisfied, the frequency with a relatively small number of modes and an excitation conditions should be selected. A large number of modes will cause the energy of the excitation signal to be dispersed, which will cause the signal-to-noise ratio of the detection signal to decrease and affect the detection sensitivity.

By considering the number of modes and group velocity difference, the frequency selection factor α is defined as follows

$$\alpha = \frac{n_{\max}}{n_i} \times \frac{\Delta v_i}{\Delta v_{\max}} \quad (28)$$

where n_i is the number of modes at the i th frequency; n_{\max} is the maximum number of modes in n_i ; Δv_i represents the difference between the speeds of the two fastest modal groups at the i th frequency; and Δv_{\max} is the maximum value in Δv_i .

Based on the above conditions, results for the group velocity dispersion curves of the rail show that four frequencies of 22.5kHz, 25kHz, 30kHz, and 40kHz satisfy the conditions. The results for each frequency selection factor are shown in Table 1.

From Table 1, at the frequency of 22.5 kHz and 30 kHz, the group velocity difference is small, which is not suitable for short-to-medium-range detection. The group velocity difference is large at the frequency of 40kHz, but there are too many modes, which is not conducive to the separation and extraction of modal signals. At the frequency of 25kHz, the number of guided wave modes is less, and the frequency selection factor is significantly greater than the other three frequencies. Therefore, 25kHz can be used as the optimal excitation frequency of rail guided waves for numerical simulations and experimental studies.

4.3 Simulation results

When the ultrasonic guided wave propagates in the rail, the dispersion characteristics of the rail will cause the signal to widen the wave packet as the propagation distance increases, and the signal amplitude will also rapidly decay, making it difficult to distinguish the signal in the time domain. Thus it is difficult to undertake long-distance detection and condition monitoring. In this paper, the sinusoidal signal modulated by the Hanning window is used as the excitation source. The energy of this signal is relatively concentrated, which can be used for long-distance propagation of the guided wave of the rail (Niu *et al.* 2019, Khalili and Khalili 2015). The signal is defined as follows

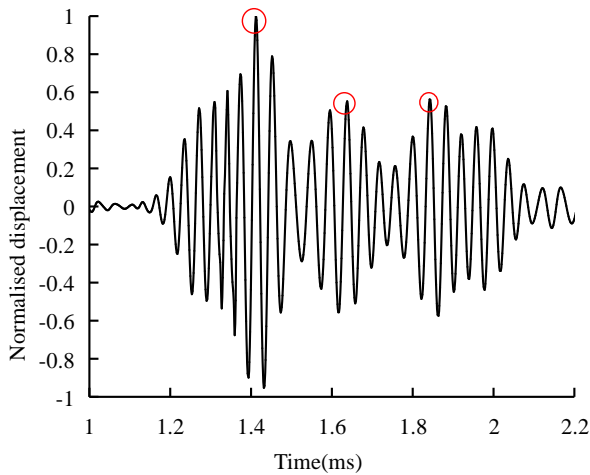


Fig. 9 The results of excitation response in the z direction

Table 2 Results for estimated group velocity

Signal peak arrival time(s)	Estimated group velocity(m/s)	Actual group velocity(m/s)	Error(%)	Corresponding guided wave mode
1.41E-03	3030	3093	1.94	Mode 12
1.64E-03	2581	2580	0.04	Mode 10
1.84E-03	2285	2260	1.11	Mode 3

$$f(t) = \left[\frac{1}{2} \left(1 - \cos \frac{2\pi f_c t}{n} \right) \times \sin(2\pi f_c t) \right] \quad (29)$$

where n is the number of signal cycles; and f_c is the centre frequency of signal.

A 25kHz, 5-cycle sinusoidal signal modulated by the Hanning window is employed here, as shown in Fig. 8. The peak value of the signal appears at 90 μ s.

In order to excite the guided wave mode 3 at the frequency of 25kHz, the excitation signals are applied at node 28 and node 71 along the x and z directions of 59R2 grooved rail, respectively. The theory introduced in Section 2.3 is used to analyze the propagation characteristics of guided waves. After the inverse Fourier transformation, the time domain waveform of the excitation response at the position at 4m away from the excitation point can be obtained, as shown in Fig. 9.

Three signal wave packets appear in Fig. 9, i.e. when excited at the positions of nodes 28 and 71 in the x and z directions, respectively, three guided wave modes will be excited in the rail. According to the time difference and propagation distance between the response signal and the excitation signal, the group velocities of three modes can be calculated, as shown in Table 2.

As can be seen from Table 2, because the cross section of the 59R2 grooved rail has a relatively complicated shape, when the excitation is performed according to the optimal excitation position of Mode 3, Mode 10 and Mode 12 are also excited together with the target Mode 3. Therefore, it is impossible to excite a relatively single target mode in the rail by means of the single point excitation-single point

reception method. A comb-shape transducer array with a number of transducers should be used for exciting the specific mode of the 59R2 grooved rail in order to effectively detect damage in the rail (Niu *et al.* 2018).

5. Conclusions

In this paper, the SAFE method is used to construct an analytical model for the 59R2 grooved rail commonly used in modern tram track structures. The dispersion curves of phase velocity and group velocity of free rails and supported rails are analyzed in detail, and the influence of rail elastic modulus on the dispersion curves of the guided waves is studied. It is found that the rail pad has a relatively little influence on the guide wave dispersion curve in the high frequency band, and a relatively large influence on the guide wave dispersion curve in the low frequency band below 4 kHz. In the high frequency band, the phase velocity is greatly affected by the rail elastic modulus, while the group velocity is more affected by the change in rail elastic modulus in the low frequency band. Based on the frequency selection factor, the optimal excitation frequency of rail guided wave is determined, and the guided wave mode, the optimal excitation point and the excitation direction suitable for on-site detection are selected by modal analysis. Finally, the sinusoidal signal modulated by the Hanning window with a central frequency of 25kHz is used as the excitation source, and the propagation characteristics of the high-frequency ultrasonic guided wave in the rail are analyzed. The simulation results are reliable with an acceptable error and demonstrate the effectiveness of the ultrasonic guided wave mode selection and excitation method proposed in this paper.

Acknowledgments

The authors are very grateful for the financial support received from the National Natural Science Foundation of China (Grant No. 51978263) and the Natural Science Key Foundation of Jiangxi Province (Grant No. 20192ACBL20008).

References

- Bartoli, I., Marzani, A., Matt, H., Scalea, F. L., and Viola, E. (2006), "Modeling wave propagation in damped waveguides of arbitrary cross-section", *J. Sound Vib.*, **295**(3), 685-707. <https://doi.org/10.1016/j.jsv.2006.01.021>.
- Cerniglia, D., Pantano, A., and Vento, M. A. (2012), "Guided Wave Propagation in a Plate Edge and Application to NDI of Rail Base", *J. Nondestructive Evaluation*, **31**(3), 245-252. <https://doi.org/10.1007/s10921-012-0139-7>.
- Chen, H. P. (2018), *Structural Health Monitoring of Large Civil Engineering Structures*, John Wiley and Sons Limited, Oxford, United Kingdom.
- Chen, H. P., Zhang, C., and Huang, T. L. (2017), "Stochastic modelling fatigue crack evolution and optimum maintenance strategy for composite blades of wind turbines", *Struct. Eng. Mech.*, **63**(6), 703-712. <https://doi.org/10.12989/sem.2017.63.6.703>.

- Coccia, S., Bartoli, I., Marzani, A., Scalea, F.L.D., Salamone, S., and Fateh, M. (2011), "Numerical and experimental study of guided waves for detection of defects in the rail head", *NDT E International*, **44**(1), 93-100. <https://doi.org/10.1016/j.ndteint.2010.09.011>.
- Duan, W., Niu, X., Gan, T. H., Kanfoud, J., and Chen, H. P. (2017), "A Numerical Study on the Excitation of Guided Waves in Rectangular Plates Using Multiple Point Sources", *Metals*, **7**(12), 552. <https://doi.org/10.3390/met7120552>.
- Dziedzic, K., Pieczonka, L., Kijanka, P., and Staszewski, W. J. (2016), "Enhanced nonlinear crack-wave interactions for structural damage detection based on guided ultrasonic waves", *Struct. Control Health Monitor.*, **23**(8), 1108-1120. <https://doi.org/10.1002/stc.1828>.
- Gharaibeh, Y., Sanderson, R., Mudge, P., Ennaceur, C., and Balachandran, W. (2011), "Investigation of the behaviour of selected ultrasonic guided wave modes to inspect rails for long-range testing and monitoring", *Proc. Institution Mech. Eng., Part F J. Rail Rapid Transit*, **225**(3), 311-324. <https://doi.org/10.1243/09544097JRR1413>.
- Hayashi, T. (2008), "Guided wave dispersion curves derived with a semianalytical finite element method and its applications to nondestructive inspection", *Japanese J. Appl. Phys.*, **47**(5S), 3865. <https://doi.org/10.1143/jjap.47.3865>.
- Hayashi, T., Song, W. J., and Rose, J. L. (2003), "Guided wave dispersion curves for a bar with an arbitrary cross-section, a rod and rail example", *Ultrasonics*, **41**(3), 175-183. [https://doi.org/10.1016/S0041-624X\(03\)00097-0](https://doi.org/10.1016/S0041-624X(03)00097-0).
- Khalili, P., and Khalili, P. (2015), "Excitation of single-mode Lamb waves at high-frequency-thickness products", *IEEE Transactions Ultrasonics, Ferroelectrics, Frequency Control*, **63**(2), 303-312. <https://doi.org/10.1109/TUFFC.2015.2507443>.
- Li, W., Dwight, R. A., and Zhang, T. (2015), "On the study of vibration of a supported railway rail using the semi-analytical finite element method", *J. Sound Vib.*, **345**, 121-145. <https://doi.org/10.1016/j.jsv.2015.01.036>.
- Lu, C., Nieto, J., Puy, I., Melendez, J., and Martínez-Esnaola, J. M. (2018), "Fatigue prediction of rail welded joints", *J. Fatigue*, **113**, 78-87. <https://doi.org/10.1016/j.ijfatigue.2018.03.038>.
- Nilsson, C. M., Jones, C. J. C., Thompson, D. J., and Ryue, J. (2009), "A waveguide finite element and boundary element approach to calculating the sound radiated by railway and tram rails", *J. Sound Vib.*, **321**(3-5), 813-836. <https://doi.org/10.1016/j.jsv.2008.10.027>.
- Niu, X., Duan, W., Chen, H. P., and Marques, H. R. (2019), "Excitation and propagation of torsional T (0, 1) mode for guided wave testing of pipeline integrity", *Measurement*, **131**, 341-348. <https://doi.org/10.1016/j.measurement.2018.08.021>.
- Niu, X., Marques, H. R., and Chen, H. P. (2018), "Sensitivity analysis of circumferential transducer array with T(0,1) mode of pipes", *Smart Struct. Syst.*, **21**(6), 761-776. <https://doi.org/10.12989/sss.2018.21.6.761>.
- Panunzio, A. M., Puel, G., Cottureau, R., Simon, S., and Quost, X. (2018), "Sensitivity of the wheel-rail contact interactions and Dang Van Fatigue Index in the rail with respect to irregularities of the track geometry", *Vehicle Syst. Dynam.*, **56**(11), 1768-1795. <https://doi.org/10.1080/00423114.2018.1436717>.
- Ramatlo, D. A., Wilke, D. N., and Loveday, P. W. (2018), "Development of an optimal piezoelectric transducer to excite guided waves in a rail web", *Ndt E Intl.*, **2018**, 72-81. <https://doi.org/10.1016/j.ndteint.2018.02.002>.
- Rizzo, P., Cammarata, M., Bartoli, I., Scalea, F. L., Salamone, S., Coccia, S., and Phillips, R. (2010), "Ultrasonic Guided Waves-Based Monitoring of Rail Head: Laboratory and Field Tests", *Adv. Civil Eng.*, **2010**, 1-13. <http://dx.doi.org/10.1155/2010/291293>.
- Rose, J. L., Avioli, M. J., Mudge, P., and Sanderson, R. (2004a), "Guided wave inspection potential of defects in rail", *Ndt E Intl.*, **37**(2), 153-161. <https://doi.org/10.1016/j.ndteint.2003.04.001>.
- Rose, J. L., Avioli, M. J., Mudge, P., and Sanderson, R. (2004b), "Guided wave inspection potential of defects in rail", *Ndt E Intl.*, **37**(2), 153-161. <https://doi.org/10.1016/j.ndteint.2003.04.001>.
- Ryue, J., Thompson, D. J., White, P. R., and Thompson, D. R. (2008), "Investigations of propagating wave types in railway tracks at high frequencies", *J. Sound Vib.*, **315**(1-2), 157-175. <https://doi.org/10.1016/j.jsv.2008.01.054>.
- Shi, H., Zhuang, L., Xu, X., Yu, Z., and Zhu, L. (2019), "An Ultrasonic Guided Wave Mode Selection and Excitation Method in Rail Defect Detection", *Appl. Sci.*, **9**(6), 1170. <https://doi.org/10.3390/app9061170>.
- Uyar, G. G., and Babayigit, E. (2016), "Guided wave formation in coal mines and associated effects to buildings", *Struct. Eng. Mech.*, **60**(6), 923-937. <https://doi.org/10.12989/sem.2016.60.6.923>.
- Wang, R., Yu, Z.J., Zhu, L.Q. and Xu, X.N. (2018), "Multimodal guided wave fusion for estimating longitudinal thermal stress of continuously welded rail", *J. China Railway Soc.*, **40**(6), 136-143. <https://doi.org/10.3969/j.issn.1001-8360.2018.06.018>.
- Xu, C. B., Yang, Z. B., Chen, X. F., Tian, S. H., and Xie, Y. (2018), "A guided wave dispersion compensation method based on compressed sensing", *Mech. Syst. Signal Processing*, **103**, 89-104. <https://doi.org/10.1016/j.ymssp.2017.09.043>.
- Yao, W., Sheng, F., Wei, X., Zhang, L., and Yang, Y. (2017), "Propagation characteristics of ultrasonic guided waves in continuously welded rail", *Modern Physics Letters B*, **31**(19-21), 1740075. <https://doi.org/10.1142/S0217984917400759>.
- Zhang, X., Feng, N., Wang, Y., and Shen, Y. (2015), "Acoustic emission detection of rail defect based on wavelet transform and Shannon entropy", *J. Sound Vib.*, **339**, 419-432. <https://doi.org/10.1016/j.jsv.2014.11.021>.

CC